Journal of Power Sources 194 (2009) 690–696

Contents lists available at ScienceDirect

Journal of Power Sources

journal homepage: www.elsevier.com/locate/jpowsour

Characterization of the 75% $Gd_{0.8}Sr_{0.2}CoO_{3-\delta}$/25% $Ce_{0.9}Gd_{0.1}O_{2-\delta}$ composite cathode system for use in intermediate temperature solid oxide fuel cells

L.B. Kilius*, V. Krstic

Mechanical and Materials Engineering, Queen's University, Nicol Hall – 60 Union St., Kingston, Ontario, Canada K7L 3N6

ARTICLE INFO

Article history:
Received 27 April 2009
Received in revised form 9 June 2009
Accepted 9 June 2009
Available online 18 June 2009

Keywords:
Solid oxide fuel cell
Cathode
Charge transfer
Triple phase boundary
High surface area
Conductivity

ABSTRACT

The composite cathode system is examined for suitability on a $Ce_{0.9}Gd_{0.1}O_{2-\delta}$ electrolyte based solid oxide fuel cell at intermediate temperatures (500–700 °C). The cathode is characterized for electronic conductivity and area specific charge transfer resistance. This cathode system is chosen for its excellent thermal expansion match to the electrolyte, its relatively high conductivity (115 S cm^{-1} at 700 °C), and its low activation energy for oxygen reduction (99 kJ mol^{-1}). It is found that the decrease of sintering temperature of the composite cathode system produces a significant decrease in charge transfer resistances to as low as 0.25 Ω cm^2. The conductivity of the cathode systems is between 40 and 88 S cm^{-1} for open porosities of 30–40%.

1. Introduction

Traditional solid oxide fuel cells (SOFCs) are expected to operate at relatively high temperatures (800–1000 °C) where their efficiency is the highest. However, these temperatures can lead to the development of large thermal stresses which compromise the life expectancy of the materials used to fabricate the cells. Intermediate temperature SOFCs (IT-SOFCs) have been developed to operate at significantly lower temperatures (500–700 °C) in order to reduce thermal stresses. However, the electrochemical mechanisms that dictate the power output of these cells are thermally activated processes, leading to a drastic decrease in performance as temperature is decreased. In order to mitigate these losses, new material systems must be developed that have improved electrical and thermal properties.

It has been well documented that, for these intermediate temperatures, the charge transfer that occurs at the cathode–electrolyte interface restricts the performance of the cell and the oxygen must be catalytically reduced by the cathode through the following reaction:

$$\frac{1}{2}O_2 + 2e^- + V_O^{\bullet\bullet} \rightarrow O_O^X \quad (1)$$

Due to the nature of the reactants, this reaction can only take place at the triple phase boundary layer (TPB) if the cathode is a pure electronic conductor. Considering that there is only a limited TPB and thus limited number of available sites for the reaction to occur, the resistance to charge transfer is often high enough to limit the performance of the cathode [1–3]. In an attempt to reduce the interfacial losses and to increase the number of sites where oxygen reduction can occur, a number of SOFC systems which focus on mixed electronic/ionic conducting cathodes have been investigated [4–6].

Two different methods are commonly investigated to lower the interfacial losses. One of them involves the utilization of a cathode–electrolyte composite material instead of a monolithic cathode material. When electrolyte is added in sufficient amounts, ionic pathways are created connecting the bulk electrolyte with new TPB layers which extend throughout the cathode. This effectively lengthens the TPB and has been shown to reduce the interfacial losses by up to a factor of four [4]. The second method being researched involves utilizing cathode materials which display a relatively high level of ionic conduction in addition to high electronic conduction. This allows for new ionic pathways through the bulk of the cathode, extending the sites available for oxygen reduction away from the TPB [5,6].

The most frequently investigated cathode material is $La_{1-x}Sr_xMnO_{3-\delta}$ (LSM) [7,8], which has high electronic conductivity and high catalytic activity for the reduction of oxygen at elevated temperatures [9,10]. Also, LSM is an acceptable thermal expansion match to the most common SOFC electrolyte material, yttria-stabilized zirconia [11]. However, at reduced temperatures, the catalytic activity of LSM decreases, and no longer provides adequate oxygen reduction when coupled with the most commonly

* Corresponding author. Tel.: +1 613 533 2854; fax: +1 613 533 6610.
E-mail address: kilius@me.queensu.ca (L.B. Kilius).

0378-7753/$ – see front matter © 2009 Elsevier B.V. All rights reserved.
doi:10.1016/j.jpowsour.2009.06.026

used IT-SOFC electrolyte $Ce_{0.9}Gd_{0.1}O_{2-\delta}$ (CGO). For these reasons, a more suitable candidate for a cathode material must be found.

Doped cobaltite perovskites have displayed great promise for use as a cathode material for IT-SOFCs [10,12]. $A_{1-x}B_xCoO_{3-\delta}$ (A = Dy, Gd, Sm, La, B = Sr, Ca) systems exhibit electronic conductivities comparable to that of LSM, and display greater catalytic activity for the reduction of oxygen at intermediate temperatures [13,14]. These cobaltites also possess relatively high ionic conductivity (6×10^{-4} S cm^{-1} at 700 °C [15]) compared to LSM (10^{-7} to 10^{-8} S cm^{-1} at 700 °C [16]) which contributes to reduced interfacial resistance between the electrolyte and cathode by spatially extending the area of oxygen reduction away from the TPB as described earlier.

The $Gd_{1-x}Sr_xCoO_{3-\delta}$ (GSCO) system is a promising candidate cathode material. This system has high electronic conductivity when doped with Sr on the A-site and good chemical compatibility with $Ce_{0.9}Gd_{0.1}O_{2-\delta}$ [17]. However, due to the large thermal mismatch between GSCO and CGO, large stresses generated during thermal cycling lead to cell damage and even fracture [13]. It has been found by Dyck et al. [18] that the addition of CGO to GSCO in sufficient amounts can provide acceptable matching of thermal expansion between the electrolyte and the cathode without seriously compromising the electronic conductivity of the cathode.

This paper presents the conductivity and impedance analysis results of the composite cathode ceramics with the formula 75% $Gd_{0.8}Sr_{0.2}CoO_{3-\delta}$/25% $Ce_{0.9}Gd_{0.1}O_{2-\delta}$ (wt.%).

2. Experimental/materials and methods

2.1. Powder preparation

The powders used in this work were synthesized by the glycine–nitrate process (GNP) [19]. In this process, nitrates were individually dissolved into aqueous solutions, and mixed in proper stoichiometric amounts with glycine added as a fuel. The solution was heated to ignition, producing a fluffy powder in the form of ash. The ash was then calcined at various temperatures to remove any organic contamination and obtain fully crystallized powder. The compositions of the powders used in this study are listed in Table 1.

The electrolyte powders (CGO) calcined at 1050 °C were uniaxially cold-pressed at a pressure of 160 MPa into 2 mm thick pellets using 5% polyethylene glycol (PEG) as a binder. The pellets were sintered at 1350 °C for 5 h to produce electrolyte pellets with densities of over 95%.

Two cathode systems were fabricated: monolithic $Gd_{0.8}Sr_{0.2}CoO_{3-\delta}$ and a composite consisting of $Gd_{0.8}Sr_{0.2}CoO_{3-\delta}$ and 25 wt.% $Ce_{0.9}Gd_{0.1}O_{2-\delta}$ (calcined at 650 °C). Cathode powders were mixed with methanol and 5% polyethylene glycol (PEG) to form the paste that was then painted onto both flat sides of the electrolyte pellets. The painted pellets were then sintered at varying temperatures for 2 h to form symmetrical cells.

2.2. Surface area and porosity measurement

Surface area measurements were performed on all cathode compositions using BET nitrogen adsorption analysis. Post-sintered cathode samples were used in this analysis.

Table 1
Calcination temperature and particle size of the powders.

Powder	Calcination temperature (°C)/time (h)	Particle size (μm)
$Ce_{0.9}Gd_{0.1}O_{2-\delta}$	1050/2	0.444 ± .288
$Gd_{0.8}Sr_{0.2}CoO_{3-\delta}$	0900/4	1.221 ± .410
$Ce_{0.9}Gd_{0.1}O_{2-\delta}$[a]	0650/2	0.582 ± .378

[a] Electrolyte powder used in the composite cathode.

Table 2
Porosity summary of composite and monolithic cathode samples.

Sintering temperature (°C)	Cathode open porosity (%)	
	Composite	Monolithic
0950	58.3	59.6
1000	50.5	53.4
1050	43.3	45.6
1100	30.7	32.4
1200	21.5	23.2

Porosity was calculated using three separate techniques. Closed porosity was measured using the standard Archimede's method (buoyancy force balance). Open porosity was determined by calculating the water retention mass of the sample (mass difference between a dry and water saturated sample). This open porosity technique was calibrated against an alumina standard of known porosity, which provided 0.4% experimental error. The total porosity was determined by the summation of open and closed porosity, but was also verified by density determination of the samples using standard geometrical and mass measurement equipment. Samples were placed in an ultrasonic water bath for 10 min, and subsequently immersed in water for a period of at least 4 h prior to testing to ensure adequate water saturation. Open porosity values are important for this analysis, and these are given for all compositions in Table 2.

2.3. AC impedance analysis

AC impedance analysis was performed using a Solartron 1260 Gain Phase Analyser, coupled with a Solartron 1296 Dielectric Interface instrument. These tests were carried out at temperatures between 300 °C and 700 °C with sample measurements taken at every 100 °C. Measurements consisted of a complex plane response through a frequency sweep between 0.01 Hz and 10 MHz with seven samples recorded per decade of frequency. All AC impedance tests were performed at zero DC voltage bias conditions.

To model the AC impedance response of the investigated system, it is important to break down all contributing components into an equivalent circuit model so that separate losses can be quantified. The equivalent circuit model for the system being examined here is given in Fig. 1, with all components explained in detail in this section.

The complex frequency response of interfacial systems exhibits distinct depressed semi-circular arcs. This behaviour is due to a build-up of charge at the interface, creating two effects as proposed by Bauerle [20]. The first effect is known as a capacitive double layer (C_{DL}) which is the result of a charge built up on one side of the interface attracting a reverse charge on the opposing side of the interface. These charges are separated by a finite amount of space, creating a capacitive effect. The second phenomenon is the resistance to charge transfer at the interface (R_{CT}). In the case of the cathode–electrolyte interface, this resistance value directly

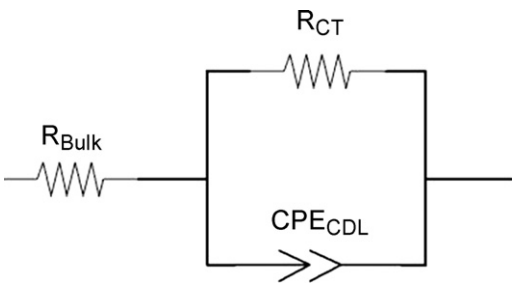

Fig. 1. AC impedance frequency response circuit model.

quantifies the losses associated with the conversion of electronic conductivity from the cathode to ionic conductivity within the electrolyte. These effects can be simulated using an equivalent circuit consisting of a capacitor C_{DL} and resistor R_{CT} in parallel.

The capacitive double layer does not exhibit pure capacitive qualities due to anisotropic variations at the cathode–electrolyte interface. Therefore, these interfacial irregularities cannot be modelled by a simple capacitor (C_{DL}). Instead a more accurate simulation of response is obtained using an imperfect capacitor, also known as a constant phase element (CPE_{CDL}). This circuit element is equivalent to that of a capacitor with its impedance raised to the exponent '*n*' [22,23].

The ohmic resistive component of the bulk electrolyte and cathode materials (R_{bulk}) is modelled by a resistor in series with the previously described parallel circuit.

It has been found that, for symmetrical cells (cathode–electrolyte–cathode), three of these semi-circular impedance arcs can form. The two high-frequency arcs, which are visible at low temperatures, are indicative of the charge transfer effects at the electrolyte grain boundaries [20,21]. The two arcs tend to disappear at higher temperatures leaving the third, low-frequency depressed arc as the sole AC impedance response. This low-frequency arc is associated with the response at the cathode–electrolyte interface. The transition temperature at which this was observed was between 500 °C and 600 °C. From this it can be inferred that at higher temperatures, the charge transfer effects which occur at electrolyte grain boundaries are minimal and do not contribute significantly to the resistance of the cell. For this reason, circuit response modelling in this study only examines the low-frequency arc which is representative of the electrode–electrolyte interface.

2.4. Conductivity testing

Conductivity tests were performed using four-point conductivity analysis. Composite cathode samples were prepared by uni-axially cold pressing at a pressure of 20 MPa into rectangular bars. Sample bars were sintered at various temperatures for 2 h to create different level of porosities. Samples were placed within a horizontal tube furnace and heated from 300 °C to 700 °C with conductivity measurements taken in 50 °C intervals. Measurements were taken using a high accuracy digital multimeter.

3. Results and discussion

3.1. Impedance analysis of the electrolyte–cathode interface

The values of charge transfer resistance were determined by modelling the electrolyte–cathode frequency response data to this circuit using standard modelling software. The determined values were adjusted for area and are summarized in Table 3 with a representative set of impedance spectra given in Fig. 2.

The presented data display a clear trend in that a reduction in sintering temperature reduces the resistance to charge transfer between the cathode and the electrolyte. Previous AC impedance studies on monolithic $Gd_{0.8}Sr_{0.2}CoO_{3-\delta}$ cathodes on $Ce_{0.9}Gd_{0.1}O_{2-\delta}$ electrolytes [18,17] generated area specific charge transfer resistance values as low as 0.2 Ω cm^2 [17] arguing that values below 8 Ω cm^2 are difficult to achieve due to insufficient adhesion between the electrolyte and the cathode at low sintering temperatures. This adhesion problem was encountered in monolithic cathode samples sintered below 1100 °C. However, in composite cathode samples, adequate adhesion was obtained for sintering the samples at temperatures <1000 °C. The increased adhesion achieved in the present system is most likely a result of the high sintering activity of the electrolyte within the composite, increasing both inter-particle bond strength and adhesion to the bulk electrolyte layer.

Fig. 3 displays the relationship between sintering temperature and charge transfer resistance. In this figure, it can be seen that the monolithic cathode displays a lower charge transfer resistance value than the composite cathode for sintering temperatures of 1050 °C and above. This is in direct contrast to the idea of adding electrolyte material to increase the number of ionic pathways to the bulk electrolyte layer to reduce charge transfer resistance. However, this effect has been shown in the literature [4] to become significant at electrolyte concentrations above 30 vol.% within the composite cathode, higher than the 27 vol.% present within the investigated composite cathode material. Thus, insufficient addition of electrolyte within the composite is concluded to be the reason for this trend. Previous studies have examined this system with higher volume fractions of electrolyte [18,25], and it was observed that for cathodes with above 25 wt.% electrolyte, the electronic conductivity of the cathode is too low. The abundance of the (electronically) insulating electrolyte phase decreases the conductivity so that it becomes the major contributing factor to cathode losses. This is the reason that higher concentrations of electrolyte were not examined in this study.

At 1000 °C, the charge transfer resistance of the composite cathode becomes less than that of the monolithic cathode. This is the temperature at which adhesion of the monolithic cathode becomes detrimental to performance as well as structural integrity. This highlights the importance of the increased sintering activity of the electrolyte material, allowing for a lower sintering temperature of the composite cathode, allowing for a further increase

Table 3
AC impedance analysis summary.

Material	Sintering temperature (°C)	Charge transfer resistance (Ω cm^2)				Activation energy (kJ mol^{-1})
		Operational temperatures (°C)				
		400	500	600	700	
100% $Gd_{0.8}Sr_{0.2}CoO_{3-\delta}$	950[a]	–	–	–	–	–
	1000	174	17.1	2.04	0.24	118.0
	1050	84	9.8	1.97	0.26	102.2
	1100	680	45.6	7.84	1.76	107.5
	1200	4992	608.1	91.90	13.01	100.1
75% $Gd_{0.8}Sr_{0.2}CoO_{3-\delta}$ 25% $Ce_{0.9}Gd_{0.1}O_{2-\delta}$	950	66.0	4.9	1.57	0.10	111.4
	1000	65.1	7.4	1.02	0.12	112.3
	1050	193.0	26.3	4.17	0.74	100.3
	1100	[b]	132.3	39.95	4.34	108.1
	1200	9382.0	725.2	82.53	13.86	118.2

[a] Poor adhesion of electrode to electrolyte.
[b] Data could not be fit to model.

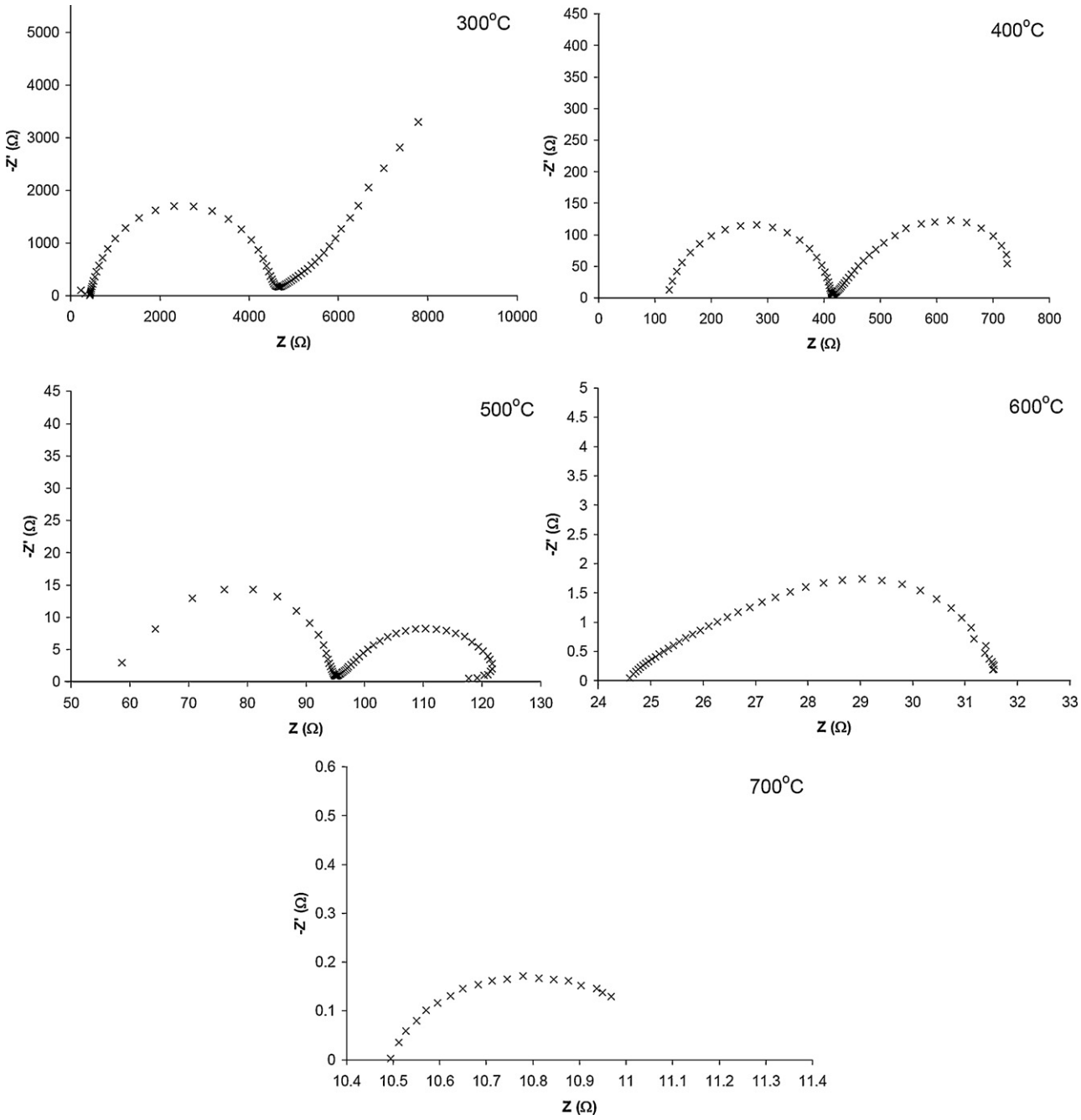

Fig. 2. Representative AC impedance spectra from the composite (75% $Gd_{0.8}Sr_{0.2}CoO_{3-\delta}$) cathode sintered at 950 °C at various operating temperatures (top right).

in performance unattainable by the less sinterable monolithic cathode.

3.2. Triple phase boundary analysis

It is believed that the reason for the drastic reduction in charge transfer resistance with sintering temperature is the increase in surface area of the bulk cathodes as the sintering temperature is decreased. A lower sintering temperature amounts to a longer effective TPB layer at which the oxygen reduction reaction can occur. Qualitative SEM image analysis of the surface of the cathodes used in AC impedance analysis tests is shown in Fig. 4 for the composite cathode and Fig. 5 for the monolithic cathode material. From these images, it is clear that the surface area of the cathode does increase as sintering temperature is decreased.

The TPB length was estimated indirectly by measured the surface area of the cathode samples using BET analysis. Since traditional chemical etching methods of measuring TPB length for LSM cathodes [3] are resisted by cobaltite cathodes, the effect of TPB on charge transfer resistance must be estimated through an indirect measurable quantity. While relationship between surface area and TPB layer is not trivial due to difficulties in describing the exact geometry of the microstructure, it is well accepted that these two parameters are closely linked [24]. Fig. 6 compares the relationship between charge transfer resistance data from Fig. 3 with cathode surface area measurements.

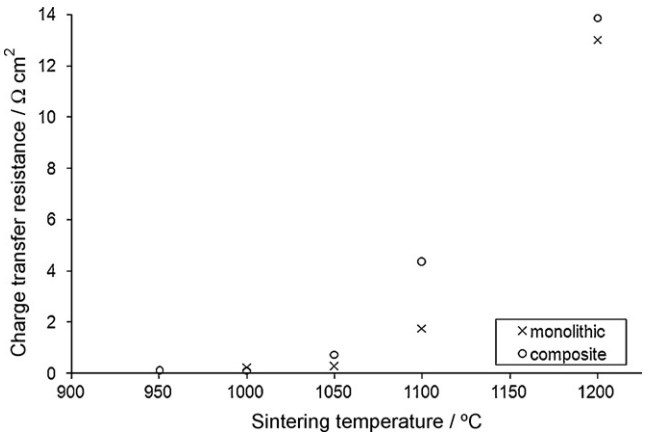

Fig. 3. The relationship between charge transfer resistance and sintering temperature for both the monolithic (100% $Gd_{0.8}Sr_{0.2}CoO_{3-\delta}$) and composite (75% $Gd_{0.8}Sr_{0.2}CoO_{3-\delta}$) cathodes examined in this study. Charge transfer resistance values were obtained at a 700 °C operating temperature.

Fig. 6 displays the trend of increasing surface area decreasing the area specific resistance, indirectly indicating that the length of the TPB plays a distinctly important role in charge transfer resistance of the cathode.

3.3. Conductivity testing

Previous studies have determined the conductivity of 75% $Gd_0Gd_{0.8}Sr_{0.2}CoO_{3-\delta}$/25% $Ce_{0.9}Gd_{0.1}O_{2-\delta}$ to be in the order of 100 S cm^{-1} at 700 °C, comparable to the standard benchmark of high density LSM cathodes at this temperature [13]. However, these values were obtained in samples containing low levels of porosity (<5%). As practical operation of SOFCs requires cathode porosity between 30% and 50%, it is necessary to determine the reduction in conductivity with the increase in porosity.

The variation of porosity in the cathode ceramics was achieved by varying the sintering temperature. The change of conductivity with sintering temperatures is shown in Fig. 7. Porosities corresponding to various sintering temperatures, along with conductivities are given in Table 3.

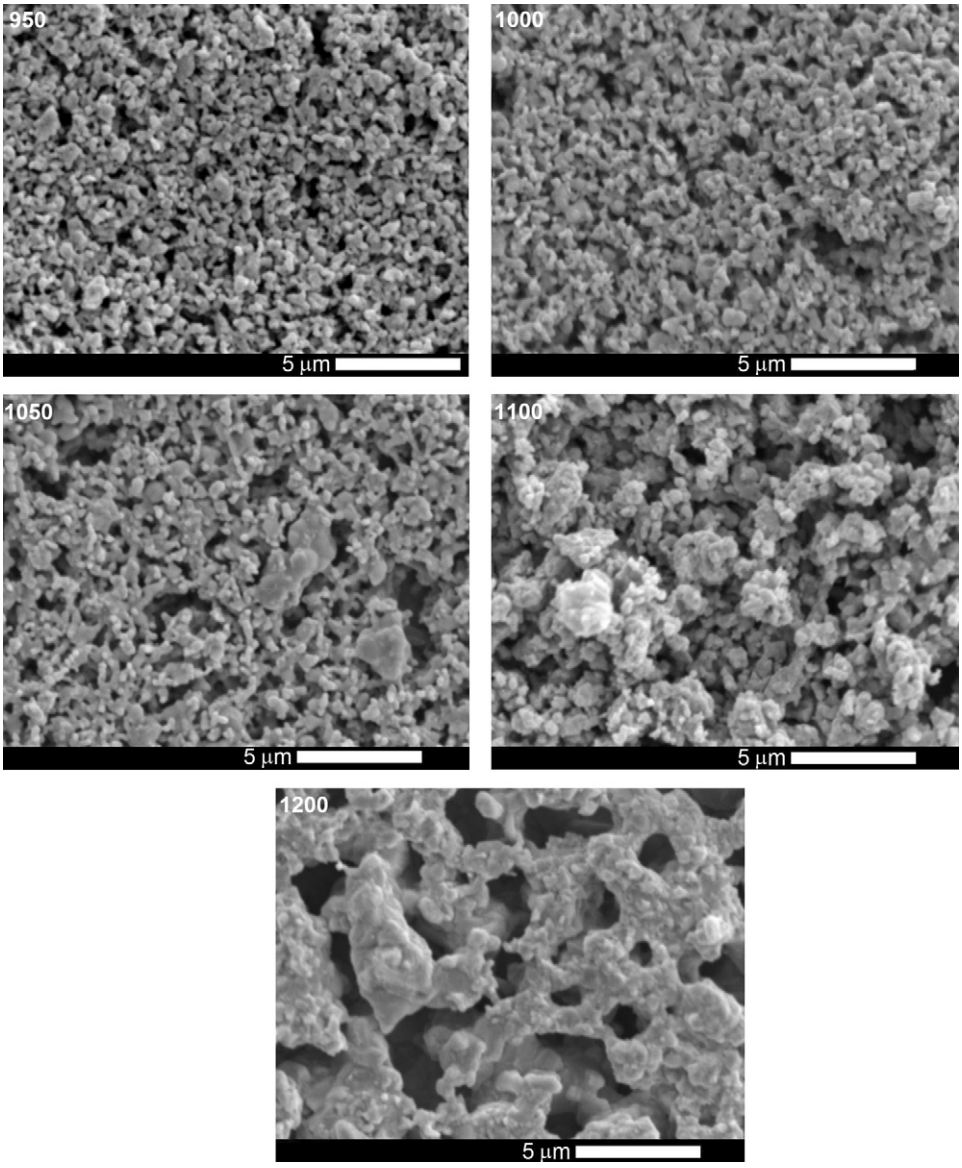

Fig. 4. SEM images of the surface of the composite cathode samples prepared for impedance testing with sintering temperatures (°C) indicated in the top left corner.

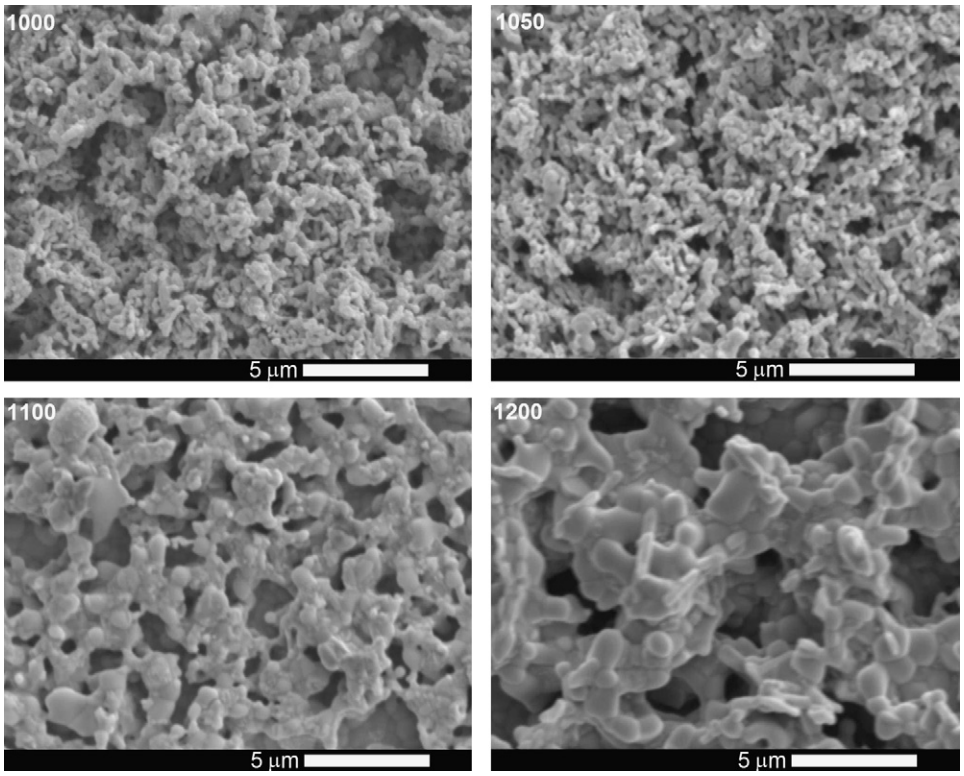

Fig. 5. SEM images of the surface of the monolithic cathode samples prepared for impedance testing with sintering temperatures (°C) indicated in the top left corner.

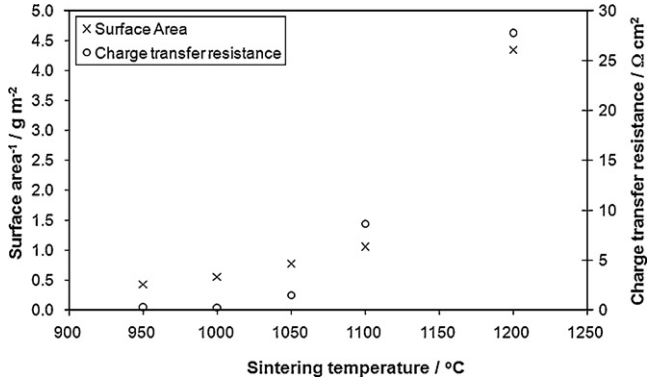

Fig. 6. Relationship between charge transfer resistance and surface area of the cathode at an operational temperature of 700 °C for the 75% $Gd_{0.8}Sr_{0.2}CoO_{3-\delta}$/25% $Ce_{0.9}Gd_{0.1}O_{2-\delta}$ cathode.

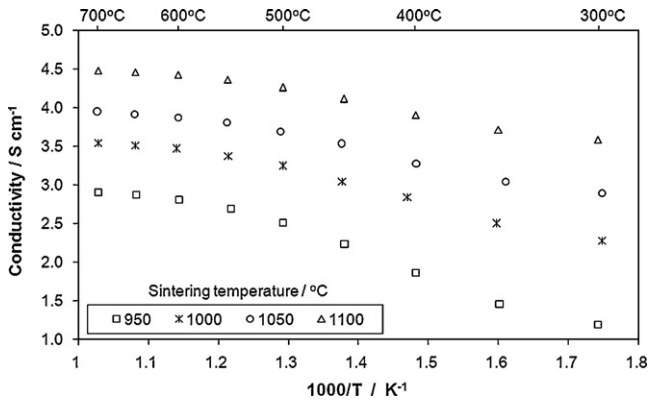

Fig. 7. Conductivity of 75% $Gd_{0.8}Sr_{0.2}CoO_{3-\delta}$/25% $Ce_{0.9}Gd_{0.1}O_{2-\delta}$ at various sintering temperatures.

Table 4
Conductivity and porosity summary of composite cathode samples.

Sintering temperature (°C)	Open porosity (%)	Conductivity (S cm^{-1})	
		700 °C	500 °C
0950	58.3	18.5	12.6
1000	50.5	34.7	25.7
1050	43.3	51.8	40.5
1100	30.7	88.4	71.3

Examination of the these results show that the conductivity values of the composite cathode at porosities of 30–50% vary between 34.7 and 88.4 S cm^{-1} at 700 °C (Table 4).

4. Conclusions

The present study shows that the newly synthesized composite cathode system consisting of 75% $Gd_{0.8}Sr_{0.2}CoO_{3-\delta}$/25% $Ce_{0.9}Gd_{0.1}O_{2-\delta}$ has high electronic conductivity and high catalytic activity for the reduction of oxygen. As previous studies have shown that this system provides a good thermal expansion match to a $Ce_{0.9}Gd_{0.1}O_{2-\delta}$ electrolyte [18], this cathode meets all the requirements for use in an IT-SOFC operating at 700 °C, identifying it as a promising candidate for use in a practical environment.

Samples sintered at 1000 °C possessed adequate adhesion between the cathode and the electrolyte with promising charge transfer resistance values of 0.12 Ω cm^2 at 700 °C. The conductivity of the composite cathode system at desired porosity levels (30–50%) was found to be between 34.7 and 88.4 S cm^{-1} at 700 °C.

Acknowledgements

The author is pleased to acknowledge the Ontario Ministry for Economic Development and Trade's Strategic Skills Initiative which has contributed to the research involved in this paper.

References

[1] B.C.H. Steele, Solid State Ionics 75 (1995) 157.
[2] B.C.H. Steele, Solid State Ionics 86–88 (1996) 1223.
[3] M. Kuznecov, P. Otschik, N. Trofimenko, K. Eichler, Russian Journal of Electrochemistry 40 (2004) 1162.
[4] V. Dusastre, J.A. Kilner, Solid State Ionics 126 (1999) 163.
[5] S.B. Adler, J.A. Lane, B.C.H. Steele, Journal of the Electrochemical Society 143 (1996) 3554.
[6] T. Horita, K. Yamaji, N. Sakai, Y. Xiong, T. Kato, H. Yokokawa, T. Kawada, Journal of Power Sources 106 (2002) 224.
[7] N.Q. Minh, T. Takahashi, Science and Technology of Ceramic Fuel Cells, Elsevier, Amsterdam, 1995.
[8] A.J. McEvoy, Journal of Materials Science 36 (2001) 1087.
[9] K. Miriam, I. Riess, D.S. Tannhauser, R. Langpape, F.J. Rohr, Journal of Solid State Chemistry 42 (1982) 125.
[10] Y. Takeda, R. Kanno, M. Noda, Y. Tomida, O. Yamamoto, Journal of the Electrochemical Society 134 (1987) 2656.
[11] H. Ullmann, N. Trofimenko, F. Tietz, D. Stover, A. Ahmad-Khanlou, Solid State Ionics 138 (2000) 79.
[12] Y. Takeda, H. Ueno, N. Imanishi, O. Yamamoto, N. Sammes, M.B. Phillipps, Solid State Ionics 86–88 (1996) 1187.
[13] M.B. Phillipps, N.M. Sammes, O. Yamamoto, Solid State Ionics 123 (1999) 131.
[14] H.Y. Tu, Y. Takeda, N. Imanishi, O. Yamamoto, Solid State Ionics 100 (1997) 283.
[15] H.-D. Wiemhofer, H.-G. Bremes, U. Nigge, Solid State Ionics 175 (2004) 93.
[16] A. Endo, M. Ihara, H. Komiyama, K. Yamada, Solid State Ionics 86–88 (1996) 1191–1195.
[17] J.M. Ralph, C. Rossignol, R. Kumar, Journal of the Electrochemical Society 150 (2003) A1518.
[18] C.R. Dyck, Z.B.H. Yu, V.D. Krstic, Solid State Ionics 171 (2004) 17.
[19] L.A. Chick, L.R. Pederson, G.D. Maupin, J.L. Bates, L.E. Thomas, G.J. Exarhos, Materials Letters 10 (1990) 6.
[20] J.E. Bauerle, Journal of Physics and Chemistry of Solids 30 (1969) 2657.
[21] M.J. Verkerk, A.J. Burggraaf, Journal of Materials Science 17 (1982) 3113.
[22] G. Chiodelli, P. Lupotto, Journal of the Electrochemical Society 138 (1991) 2703.
[23] J.R. Macdonald (Ed.), Impedance Spectroscopy—Emphasizing Solid Materials and Systems, Wiley–Interscience, New York, USA, 1987.
[24] S. Adler, Chemical Reviews 104 (2004) 4791.
[25] C.R. Dyck, MSc. Thesis, Queen's University, Kingston, Canada, 2003.